Met. Mater. Int., Vol. 17, No. 5 (2011), pp. 853~856
doi: 10.1007/s12540-011-1025-z Published 27 October 2011

Formation and crystallization of an amorphous $Al_{80}Fe_{10}Ti_5Ni_3B_2$ alloy

M. Tavoosi*, M. H. Enayati, and F. Karimzadeh

Department of Material Engineering, Nanotechnology and Advanced Material Institute
Isfahan University of Technology (IUT), Isfahan 84156-83111, Iran

(received date: 27 September 2010 / accepted date: 26 May 2011)

In this study, we investigated the crystallization behavior of an $Al_{80}Fe_{10}Ti_5Ni_3B_2$ amorphous alloy (obtained by mechanical alloying) using X-ray diffraction (XRD), transition electron microscopy (TEM), and differential thermal analysis (DTA) techniques. The obtained results show that an amorphous phase formed during mechanical alloying (for 40 h) of the Al-10%Fe-5%Ti-3%Ni-2%B powder mixture. It was found that the $Al_{80}Fe_{10}Ti_5Ni_3B_2$ amorphous alloy exhibits one-stage crystallization when heated (amorphous to $Al_{13}Fe_4$, Al_5Fe_2 and AlFe intermetallic phases). The activation energy for the crystallization, evaluated from the Kissinger equation, was about 242 ± 5 kJ/mol. We also discuss kinetic parameters such as the Avarmi exponent and reaction order (*n*). The results show that only one three-dimensional diffusion-controlled growth mechanism was working during the amorphous-glass process of the investigated glass.

Keywords: amorphous materials, mechanical alloying/milling, phase transformation, thermal analysis

1. INTRODUCTION

Alloys with Al content of 80 % to 90 % have attracted considerable attention since 1987 due to their combination of good ductility and high strength. Among the aluminum alloys, Al-Fe systems are of technological interest due to their advantageous properties, in particular a high specific strength, high specific stiffness, good strength at intermediate temperatures, and excellent corrosion resistance at elevated temperatures under oxidizing, carburizing, and sulfidizing atmospheres [1-7]. A new class of Al-base alloys that has received a great deal of attention over the last few years is amorphous as well as nanocrystalline [8]. Amorphous alloys can have an unusual combination of properties such as high strength, good ductility, high fracture toughness, and good corrosion resistance [8-11].

It has been shown that these types of alloys can be prepared by using either melt spinning or mechanical alloying (MA) techniques. Mechanical alloying is a widely used processing route for synthesis of a variety of phases, mainly non-equilibrium ones.

Metallic glasses are kinetically metastable materials. It is generally known that high strength and good bend ductility of melt-spun amorphous alloys are lost by annealing-induced crystallization. However, in the last decade, a substantial increase in strength has been reported in a number of multiphase nanocrystalline alloys. The bulk of amorphous alloys with nanocrystalline dispersoids (nanocrystals dispersed in amorphous matrix) have been reported to have more improved strength than fully amorphous alloys [12]. Hence, the kinetics of crystallization of an amorphous system is an important subject for study since it provides new opportunities for structure control by innovative alloy design and processing techniques.

This study proposed to fabricate an amorphous $Al_{80}Fe_{10}Ti_5Ni_3B_2$ alloy by mechanical alloying of mixed elemental powders. We studied the thermal behavior of the milling products as well as structural and phase changes taking place during MA and heating of the milling products. More accurate values for the activation energies of crystallization in addition to other kinetic parameters (Avrami exponent, *n*), which describe the mechanism of the crystallization for the $Al_{80}Fe_{10}Ti_5Ni_3B_2$ amorphous alloy, were also investigated.

2. EXPERIMENTAL PROCEDURE

The powders of Al (99 %), Fe (99.9 %), Ti (99 %), Ni (99.99 %), and B (98 %) were used as raw materials. The elemental powders with composition of $Al_{80}Fe_{10}Ti_5Ni_3B_2$ were mechanically alloyed in a planetary ball mill under argon atmosphere. MA was carried out in a steel container at room temperature. The rotation speed of 250 rpm and ball to powder ratio of 10:1 was employed. The process control agent (PCA) used was a 1 wt.% stearic acid powder

*Corresponding author: m.tavoosi@ma.iut.ac.ir

supplied by Merck.

X-ray diffractometery was used to follow the structural changes of powders during milling and subsequent annealing. A Philips diffractometer (40 kV) with Cu K radiation (λ = 0.15406 nm) was used for XRD measurements. The XRD patterns were recorded in the 2θ range of 20° to 100° (step size 0.03°, time per step 1 s).

The microstructure of produced amorphous powder was investigated by high-resolution transmission electron microscopy (HRTEM, Jeol-JEM-2010), and selected area diffraction pattern (SADP) analysis operated at an accelerating voltage of 200 kV resolution of 0.19 nm.

Differential thermal analysis was also conducted to study the thermal stability of the produced amorphous alloy using a Reometric STA 1500 differential thermal analyzer. The samples were placed in Al_2O_3 pans and heated in a dynamic Ar atmosphere up to 1200 °C at different heating rates of 10 °C/min, 20 °C/min and 30 °C/min.

3. RESULTS AND DISCUSSION

Figure 1 shows the XRD patterns of the Al-10 %Fe-5 %Ti-3 %Ni-2 %B powder mixture after various milling times. The XRD results demonstrate that with increased milling time, the intensity of the alloying elements diffraction peaks decreases progressively. These changes suggest that these elements dissolve in an Al matrix and an Al solid solution forms during this stage of the process. Another feature that can be seen in this pattern is a broadening of the Al diffraction peaks due to the reduction in grain size and the increase in lattice strain. In the XRD pattern obtained after 10 h of milling, one can see broad Al based solid solution peaks and a small broad halo due to an amorphous component seeming to overlap the most intense peak. After 40 h of MA, the Al peaks vanish completely and only an amorphous halo is visible (this is in agreement with the TEM results which are presented in Fig. 2).

The DTA curves of amorphous $Al_{80}Fe_{10}Ti_5Ni_3B_2$ at different heating rates are given in Fig. 3. As the heating rate

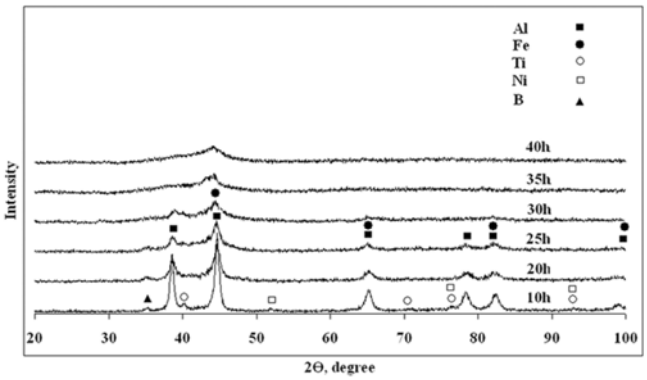

Fig. 1. The XRD patterns of Al-10%Fe-5%Ti-3%Ni-2%B powder mixture after various milling times.

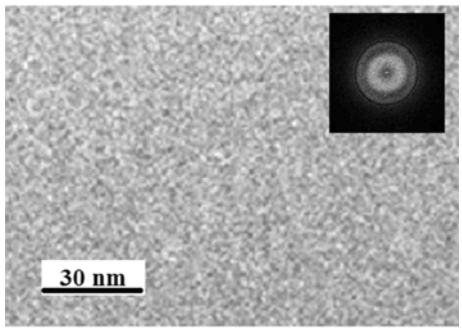

Fig. 2. TEM image of the Al-10%Fe-5%Ti-3%Ni-2%B powder mixture after 40 h of MA.

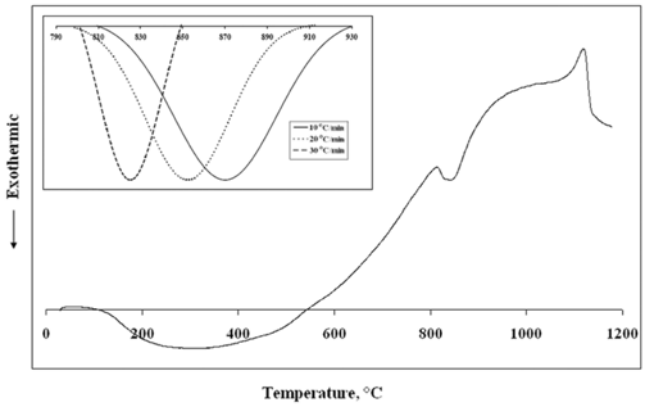

Fig. 3. DTA curves of amorphous $Al_{80}Fe_{10}Ti_5Ni_3B_2$ alloy at different heating rates.

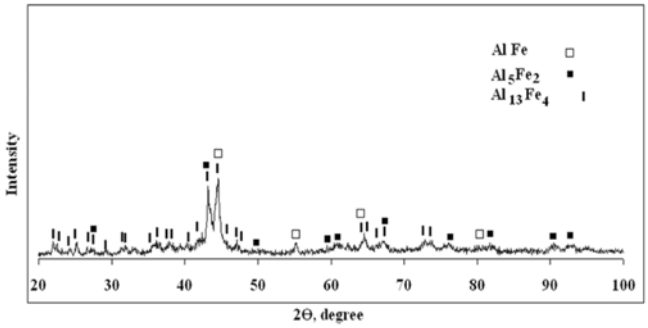

Fig. 4. The XRD pattern of amorphous $Al_{80}Fe_{10}Ti_5Ni_3B_2$ alloy annealed at temperature 1000 °C for 20 min.

increases, the crystallization peak shifts to high temperatures. There is only one exothermic peak observed in the samples in the temperature range of 800 °C to 850 °C; it is the crystallization of the amorphous phase which then transforms into the $Al_{13}Fe_4$, Al_5Fe_2 and AlFe intermetallics phase. This can be identified by the XRD patterns of samples annealed at 1000 °C for 20 min, as shown in Fig. 4. Meanwhile, the endothermic peak in Fig. 3 (at 1130 °C) is related to the melting of the produced alloy.

The effective activation energy of crystallization can be estimated following the Kissinger equation [13,14]:

$$\ln\frac{\beta}{T^2} = \frac{E}{RT} + \text{const} \quad (1)$$

where T stands for the peak temperature of the exothermic peak, β is the heating rate, R is the gas constant, and E is the effective activation energy of crystallization. The Kissinger plot $\ln(\beta/T^2)$ versus 1/T consists of approximately straight lines. Based on the slope of the Kissinger plots, the effective activation energy of crystallization, estimated from the peak temperature of exothermic peaks, is 242 ± 5 kJ/mol.

The area under the DTA curve is directly proportional to the total amount of alloy crystallized. The volume fraction (α) of the sample transformed into crystalline phase during the crystallization event has been obtained from the DTA curves (Fig. 3) as a function of temperature (T) by means of the partial area method. The plots of α versus T at different heating rates are shown in Fig. 5. Their shapes are a typical sigmoid curve, which appears frequently in the literature [15-17]. The sigmoid plot exhibits the bulk crystallization and excludes the chance of surface crystallization [17].

The local activation energy of crystallization, which changes with crystallization fraction, can be determined by the Flynn-Wall-Ozawa method [18-20]:

$$\log\beta = \log\frac{AE(x)}{g(x)R} - 2.315 - \frac{0.457E(x)}{RT}, \quad (2)$$

where A is the pre-exponential factor and E(x) is the local activation energy of crystallization. Here β, R, and T have known meanings, and $g(x)$ is a function determined by the fraction of crystallization. Equation 2 is used to determine the local activation energy for given values of the crystallization fraction. The local activation energy of crystallization $E(x)$ for different crystallization fraction can be calculated from a log β versus 1000/T plot.

We used the Flynn-Wall-Ozawa method to estimate the local activation energy by analyzing the data in Fig. 5; the

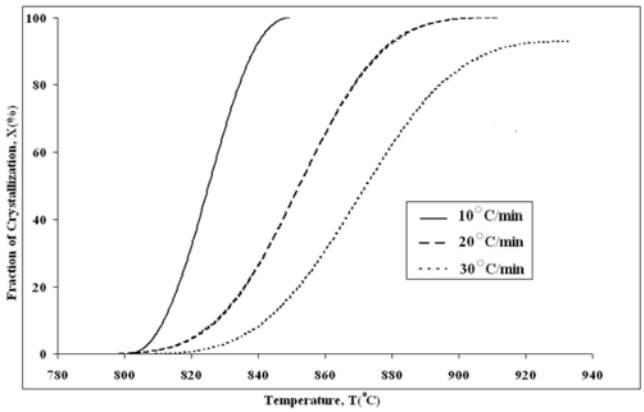

Fig. 5. The relationship between the crystallization fraction (x) and temperature (T) in amorphous $Al_{80}Fe_{10}Ti_5Ni_3B_2$ alloy.

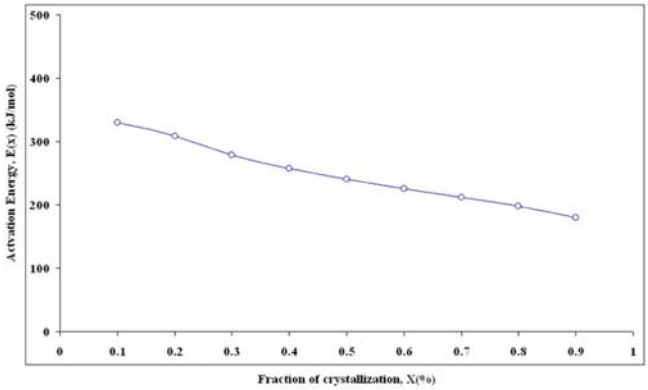

Fig. 6. Local activation energies of crystallization versus the crystallization fraction.

results are shown in Fig. 6. It can be seen that the local activation energy slightly decreases with the development of crystallization. It indicates that the process of crystallization is easier as the temperature or crystallization fraction increases.

As pointed out by Ozawa [21], crystallization kinetics can be determined by employing isochronal differential thermal analyses (DTA) and fitting to the Johnson, Mehl, and Avrami (JMA) model

$$\ln[-\ln(1-x)] = \ln\chi(T) - n\ln\beta, \quad (3)$$

where n is an Avrami exponent. We obtained the following formula after transformation of Eq. 3 at some temperature T:

$$\left.\frac{d\{\ln[-\ln(1-x)]\}}{d\ln\beta}\right|_T = -n \quad (4)$$

The Avrami exponent n can be determined from -ln[-ln(1-x)] versus lnβ plot. The results are shown in Fig. 7, from which one can see that the Avrami exponent n (in the range of $3 < n < 3.7$) decrease as temperature increases. The Avrami exponent gives detailed information on the nucleation and growth mechanism. Ranganathan and Heimendahl [22] suggested that the Avrami exponent could be expressed as:

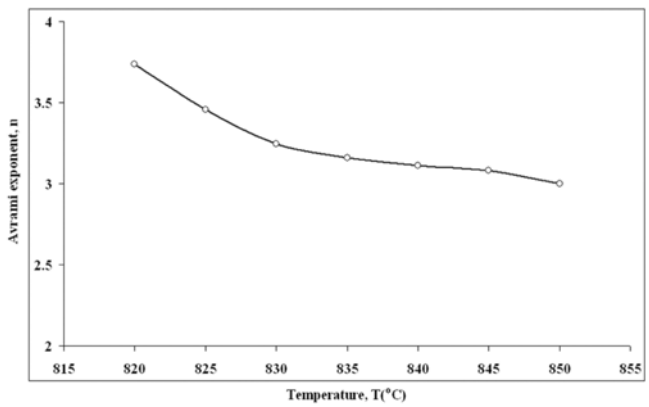

Fig. 7. Avrami exponent versus temperature.

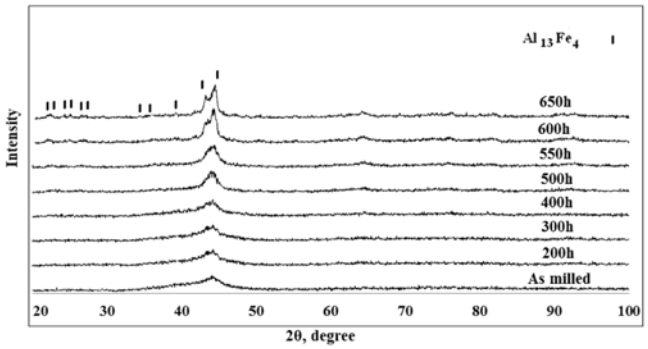

Fig. 8. The XRD patterns of the $Al_{80}Fe_{10}Ti_5Ni_3B_2$ amorphous phase after annealing at 200 °C, 300 °C, 400 °C, 500 °C, 550 °C, 600 °C, and 650 °C for 1 h.

$$n = a + bc \quad (5)$$

where a is the nucleation index, which can range from 0 to 1 ($a = 0$ for a nucleation rate of zero, $0 < a < 1$ for a nucleation rate decreasing with time, $a = 1$ for a constant nucleation rate and $a > 1$ for an increasing nucleation rate), b is the dimension of the growth (with values 1, 2, or 3 for one-, two-, three dimensional growth, respectively), and c is the growth index ($c = 1$ for interface-controlled growth and $c = 0.5$ for diffusion controlled growth). As for the $Al_{80}Fe_{10}Ti_5Ni_3B_2$ amorphous alloy, it can be found that the value of index a was more than 1, implying an increasing nucleation rate, the index b was equal to 3, corresponding to a 'sphere-type growth', and the value of index c was equal to 0.5, meaning a diffusion controlled growth. This suggests that the crystallization of the $Al_{80}Fe_{10}Ti_5Ni_3B_2$ amorphous alloy occurred with an increased nucleation rate and was governed by a three-dimensional diffusion-controlled growth.

In order to investigate the thermal stability and structural changes of produced amorphous alloy under crystallization temperature, the as-milled powder particles (for 40 h) were annealed at several temperatures for 1 h. The XRD patterns of as-milled and annealed samples at 200 °C, 300 °C, 400 °C, 500 °C, 550 °C, 600 °C and 650 °C are presented in Fig. 8.

Analysis of the XRD patterns in Fig. 8 reveal that after annealing the powder mixture at temperatures below 400 °C, structural relaxation and stress relief processes were the only considerable changes that occurred in the amorphous phase, and no evidence of crystallization was found in the XRD patterns. In contrast to the above, by annealing the samples above 400 °C (under crystallization temperature), the $Al_{13}Fe_4$ intermetallic phase precipitated from the amorphous matrix. As seen in Fig. 8, the intensity of the $Al_{13}Fe_4$ intermetallic peaks in the XRD patterns increases with annealing temperature. It is indicated that the volume fraction of the $Al_{13}Fe_4$ intermetallic phase that precipitated from the amorphous matrix increases at higher temperatures.

4. CONCLUSIONS

We investigated the crystallization kinetics of an $Al_{80}Fe_{10}Ti_5Ni_3B_2$ amorphous alloy by using a non-isothermal DTA analysis method, and summarize our main results as follows. Amorphous $Al_{80}Fe_{10}Ti_5Ni_3B_2$ alloy is obtained by mechanical alloying. The crystallization process of the $Al_{80}Fe_{10}Ti_5Ni_3B_2$ amorphous alloy is a one-stage mode, which corresponds to the intermetallic compounds $Al_{13}Fe_4$, Al_5Fe_2 and AlFe. The activation energy for the crystallization evaluated from the Kissinger equation is 242 ± 5 kJ/mol by using the peak temperature of the exothermic reaction. The Avarmi exponent or reaction order (n) indicates that the nucleation rate increases with time and crystallization is governed by a three-dimensional diffusion-controlled growth.

REFERENCES

1. A. Inoue, M. Yamamoto, H. M. Kimura, and T. Masumoto, *J. Mater. Sci. Lett.* **6**, 194 (1987).
2. A. Inoue, K. Ohetera, A. Tsai, and T. Masumoto, *J. Appl. Phys.* **27**, 479 (1988).
3. Y. H. Kim and A. Inoue, *Mater. Trans. JIM*, **31**, 747 (1990).
4. S. Enzo, G. Mulas, and R. Frattini, *Mater. Sci. Forum* **269-272**, 385 (1988).
5. F. Cardellini, V. Contini, R. Gupta, G. Mazzone, A. Montone, A. Perin, and G. Principi, *J. Mater. Sci.* **33**, 2519 (1988).
6. Y. Zou, S. Saji, and T. Kusabiraki, *Mater. Res. Bull*, **37**, 123 (2002).
7. M. Krasnowski, A. Grabias, and T. Kulik, *J. Alloys Compd.* **424**, 119 (2006).
8. A. Inoue, *Prog. Mater. Sci.* **43**, 365 (1998).
9. H. Gleiter, *Nanostruct. Mater.* **1**, 1 (1992).
10. G. W. Nieman, J. R. Weertman, and R. W. Siegel, *Nanostruct. Mater.* **1**, 185 (1992).
11. C. Suryanarayana, *Prog. Mater. Sci.* **46**, 1 (2001).
12. F. Zhou, R. Luck, M. Scheffer, D. Lang, and K. Lu, *J. Non-Cryst. Solid.* **250-252**, 704 (1999).
13. H. E. Kissinger, *Anal. Chem.* **29**, 1702 (1957).
14. T. Akahira and T. Sunose, *Res. Report Chiba Inst. Technol.* **16**, 22 (1971).
15. H. R. Wang, Y. L. Gao, Y. F. Ye, G. H. Min, Y. Chen, and X. Y. Teng, *J. Alloy. Compd.* **353**, 200 (2002).
16. C. Popescu, *Thermochim. Acta* **285**, 309 (1996).
17. A. Pratap, K. N. Lad, T. L.S. Rao, P. Majmudar, and N. S. Saxena, *J. Non-Cryst. Solids* **345-346**, 178 (2004).
18. J. H. Flynn and L. A. Wall, *J. Res. Nat. Bur. Stand. A: Phys. Chem.* **70A**, 487 (1966).
19. J. H. Flynn and L. A. Wall, *Polym. Lett.* **4**, 323 (1966).
20. T. Ozawa, *Bull. Chem. Soc. Jpn.* **38**, 1881 (1965).
21. T. Ozawa, *Polymers* **12**, 150 (1971).
22. S. Ranganathan and M.V. Heimendahl, *J. Mater. Sci.* **16**, 2401 (1981).